ANALYSIS OF FULL WAVEFORM LIDAR DATA FOR TREE SPECIES CLASSIFICATION

Josef Reitberger [a, *], Peter Krzystek [a], Uwe Stilla [b]

[a] Dept. of Geoinformatics, Munich University of Applied Sciences, 80333 Munich, Germany
(reitberger, krzystek)@fhm.edu
[b] Photogrammetry and Remote Sensing, Technische Universitaet München, 80290 Munich, Germany
stilla@tum.de

Commission III, WG III /3

KEY WORDS: LIDAR, analysis, segmentation, classification, forestry, vegetation

ABSTRACT:

The paper describes an approach to tree species classification based on features that are derived by a waveform decomposition of full waveform LIDAR data. Firstly, 3D points and their attributes are extracted from the waveforms, which yields a much larger number of points compared to the conventional first and last pulse techniques. This is caused by the detailed signal analysis and the possibility to detect multiple pulse reflections. Also, constraints are embedded into the mathematical model of the decomposition to avoid erroneous 3D points caused by the system electronics. Secondly, special tree saliencies are proposed, which are computed from the extracted 3D points. Subsequently, an unsupervised tree species classification is carried out using these saliencies. The classification, which groups the data into two clusters (deciduous, coniferous), leads to an overall accuracy of 80 % in a leaf-on situation. Finally, the results are shortly discussed.

1. INTRODUCTION

Remote sensing techniques have great potential to automatically derive forest structures and parameters that are captured so far in time consuming campaigns with considerable manpower. Microwave sensors, optical sensors, and laser sensors record data that contain inherent object information as a result of the interaction of the sensor specific wavelength with the forest.

Microwave sensor systems have the advantage to penetrate the forest structure, are weather independent and less expensive. Primarily due to the complex back scattering mechanism the application of both InSAR and PolInSAR in forest is restricted to the extraction of overall parameters like the biomass parameter and the generation of a crude DSM (Aulinger et al., 2005). SAR tomography does not depend on assumptions about the spatial forest structure like PolInSAR and represents a true 3D mapping technique, however is far from practicability (Reigber, 2001).

Optical sensors map at a high ground sample distance the canopy surface in particular bands depending on the spectral resolution. The measured pixel value represents only the intensity that is directly reflected from the canopy surface element. The way the sun light photons are interacting with the entire tree structure is not recorded. Thus, spatial forest parameters can only be derived indirectly from surface parameters like the crown diameter. So far, most of the applications with optical sensors aimed at medium and small scale forest inventory (Hyyppä et al., 2000). New digital aerial cameras providing multi-spectral images with high geometrical resolution are promising. DSM generation and tree height determination based on image correlation has been reported recently (Baltsavias et al., 2006). Also, tree species classification was demonstrated using the DMC digital aerial camera (Persson et al., 2004).

LIDAR comprises several advantages for forest applications. The laser beam may penetrate the forest structure, and the technique provides 3D information at a high point density and intensity values at a specific wavelength. Since over a decade conventional LIDAR - recording the first and last pulse - has been widely used to successfully retrieve forest parameters (Hyyppä et al., 2004; Heurich et al., 2004). Holmgren (2003) shows that single trees like Norway Spruce and Pine can be delineated and classified using highly dense LIDAR data in forest structures which are typical for Scandinavian forests. However, conventional LIDAR data do not provide desirable forest features like young regeneration due to the limited range resolution and penetration rate.

A conventional LIDAR system has limitations concerning the number of recordable pulse reflections. Also, the information about the reflecting object and its geometric and physical characteristics is not registered. New full waveform scanners overcome this drawback, since they record the entire laser pulse echo as a function of time. Therefore, detailed information about the geometric and physical characteristics of the tree structure can be derived and used to retrieve more sophisticated and precise forest structures.

The presented work is focused on automated extraction of forest parameters. The overall goal is to replace time consuming and expensive methods of forest inventory by new techniques exploiting LIDAR data from new full waveform scanners. In this paper we report on an approach to waveform decomposition and tree species classification using full waveform LIDAR data.

* Corresponding author.

The paper is structured by five sections. Section 2 describes the decomposition of the waveform based on a robust adjustment scheme. Section 3 presents the approach to tree species classification. Section 4 shows results obtained from full waveform data collected in fall 2004 by the TopEye MK II system in the Bavarian Forest National Park. Finally, the results are discussed with conclusions in section 5 and 6.

2. DECOMPOSITION OF FULL WAVEFORM DATA

2.1 General Remarks

Generally, the recorded waveform is influenced by the transmitted pulse, the atmosphere and the object. Wagner et al. (2003) present a theoretical model for the interaction of a single laser beam with topographic targets like leaves, power lines, roofs and trees. For simplification, it neglects the mitigation of the laser pulse when travelling through a tree volume. Several approaches to decompose a single waveform have been published. Hofton et al. (2000) suggest to fit several Gaussian distribution functions in a nonlinear least squares adjustment to the waveform. Likewise, Jutzi and Stilla (2005) model the waveform with Gaussians by a Gauss-Newton method. Finally, Persson et al. (2005) introduced another method based on the Expectation-Maximation algorithm.

2.2 Approach

Our approach to decompose the full waveform data is based - similar to Hofton et al. (2000) - on the assumption, that the transmitted pulse is of Gaussian type and the registered waveform is composed from several single laser returns that are also of Gaussian type. Thus, we model the waveform *w(t)* with a sum of single Gaussian distribution functions

$$w(t) = \varepsilon + \sum_{m=1}^{N_p} A_m \exp\left[-\frac{(t-t_m)^2}{2\sigma_m^2}\right] \qquad (1)$$

with

N_P : Number of peaks — A_m: Amplitude of the mth peak

ε : Bias (noise level) — t_m : Time position of the mth peak

σ_m : half width of the mth peak

The nonlinear observation equation (1) is linearized with respect to the unknown model parameters $x^T = (\varepsilon, A_m, t_m, \sigma_m)$ ($m = 1, N_p$). A standard least squares adjustment estimates the unknown variables x by the normal equation system

$$(A^T PA)x = A^T Pl \qquad (2)$$

with A as the design matrix, P as the weighting matrix and l as the observation vector.

Since initial experiments showed that the standard least squares adjustment cannot clearly extract single returns from the registered waveform in case of overlaying return pulses, the Levenberg-Marquardt (LM) (Levenberg, 1944; Marquardt, 1963) iteration scheme was added by replacing the normal equation matrix $N = A^T PA$ in (2) with augmented normal equations N', where

$$N'_{ii} = (1+\lambda)N_{ii} \text{ and } N'_{ij} = N_{ij} \text{ for } i \neq j \,. \qquad (3)$$

The damping factor λ is initially set to 10^{-3} and is scaled down by the factor 10 as long as the solving of the normal equations shows a good convergence. In case of a divergence λ is multiplied by 10 and the normal equations are solved again. This process continues until the normal equation converges significantly.

The initial values $\varepsilon^0, A_m^0, t_m^0, \sigma_m^0$ for the unknown parameters are derived as follows. The median of the waveform *w(t)* is used as starting value for ε, i.e. $\varepsilon^0 = median(w(t))$. Initial values A_m^0 for the amplitudes and t_m^0 for the time positions of the peaks are found by smoothing the original signal by a 1x3 Gaussian filter and computing the first derivative of the smoothed curve. Possible time positions t_m^0 of a peak are zero crossings of the first derivative of *w(t)*. In order to distinguish between real returns and noise a threshold $C_{threshold}$ based on the median absolute deviation *MAD=median(|w(t) - median(w(t))|)* of the waveform *w(t)*, which is a measure of dispersion of a distribution about the median (Rousseeuw and Leroy, 1987), is calculated. The threshold $C_{threshold}$ is set to

$$C_{threshold} = median(w(t) + 3 \cdot 1.4826 \cdot MAD) \qquad (4)$$

in order to achieve consistency with the standard deviation for asymptotical normal distributions. We just select potential local maxima with amplitudes larger than the threshold $C_{threshold}$. The initial values σ_m^0 are set to 0.25 m, which is equivalent to the standard deviation of the transmitting pulse (pulse length 5 ns) assuming that it is of Gaussian type.

The internal accuracy of the estimated parameters are derived from the inverse normal equation matrix N^{-1} and the sigma naught σ_0. Since the scan angle of the laser beam is rather small the standard deviation σ_{t_m} of the peak position is a good estimation of the height standard deviation of the corresponding 3D point $X_m^T = (x_m, y_m, z_m)$, i.e. $\sigma_{z_m} \approx \sigma_{t_m}$. This value is used as a quality measure after the adjustment to discard possible weak points from any further analysis based on a certain threshold.

2.3 Extraction of 3D points

The estimated time positions t_m of the Gaussian functions are used along with the starting point $X_s^T = (x_s, y_s, z_s)$, the direction vector r_s and the start time t_s of the waveform to generate the 3D points of the waveform with $X_m = X_s + (t_m - t_s)r_s \;\; (m = 1, N_p)$. Additionally, these points get the width W_m of the return pulse and the intensity related parameter I_m of the reflection as attributes. The width W_m is set to twice the estimated standard deviation σ_m, i.e. $W_m = 2 \cdot \sigma_m$. The parameter I_m is derived from the integral of the Gaussian function that can be approximated with $I_m = 2 \cdot \sigma_m \cdot A_m$ and is equivalent to the pulse energy of the reflection. Note that the parameters W_m and I_m are still sensor specific since they depend on the amplitude and pulse length of the emitted signal. Also, I_m depends on the run length s_m of the laser beam. Calibration is achieved by referencing W_m and I_m to

W^e and I^e of the emitted Gaussian pulse and correcting I_m with respect to a nominal distance s_0 according to the radar equation (Wagner et al. 2003). This leads to calibrated parameters $W_m^c = \frac{W_m}{W^e}$ and $I_m^c = \frac{I_m \cdot s_m^2}{I^e \cdot s_0^2}$, which represent additional information about the reflections of the laser beam on targets and can be used in a tree species classification.

3. TREE SPECIES CLASSIFICATION

3.1 Concept

Tree species classification is usually split up into three main steps. Firstly, individual tree crowns are delineated by a segmentation of the canopy height model, which describes the tree surface. Secondly, characteristic features of the individual trees are extracted. Thirdly, based on the extracted features tree species are classified using an appropriate classifier. So far, we have been concentrating on the second and third step and postponed the segmentation of the tree crowns.

3.2 Feature extraction

The finding of significant features describing the tree individually is a key issue in tree species classification. Assuming a given tree segment we have several waveforms intersecting the prismatic volume area from which in total *n* 3D points $X_j = \{x_j, y_j, z_j, I_j^c, W_j^c\}$ $(j = 1, n)$ can be derived containing the coordinates and the attributes of the waveform decomposition.

The salient features $S_t = \{S_g, S_i, S_I\}$ of a tree t are subdivided into three groups reflecting the outer tree geometry by S_g, the internal geometrical tree structure by S_i and the intensity-related tree structure by S_I.

For the group S_g we have developed two saliencies $S_g = \{S_g^1, S_g^2\}$. The first saliency S_g^1 consists of the parameters $\{a,b\}$ of a parabolic surface $z = a \cdot (x - x_0)^2 + b \cdot (y - y_0)^2 + z_0$ that is fitted to the 3D points of the crown shape. These points are found with a convex hull algorithm applied to the crown points. Crown points are selected from the tree segment points by discarding possible ground hits within a height bound of 1 m above the DTM and points below the crown base height h_{base}. The value for h_{base} is found by splitting the tree segment into height layers of 0.5 m and finding the lowest layer that contains more than 1% of the non-ground points. The parameters (x_0, y_0,z_0) are either adjusted or are set equal to the coordinates of the highest point found in the tree segment.

For the calculation of the second saliency S_g^2 we subdivide the tree in *l* tree layers (Figure 1). The saliency S_g^2 is composed of the mean radii $S_g^2 = \{r_k\}(k = 1, l)$ that are determined as the mean distances $r_k = \frac{1}{N_k} \sum_{i=1}^{N_k} \sqrt{(x_i - x_0)^2 + (y_i - y_0)^2}$ $(k = 1, l)$ of all N_k layer points to the tree trunk (x_0, y_0), which is set equal to the planimetric coordinates of the highest crown point (Figure 1a).

The saliency group $S_i = \{S_i^h, S_i^d\}$ describing the internal tree structure is inspired by metrics introduced for tree characterization (Naesset, 2004). The saliencies $S_i^h = \{h_k\}(k = 1, l)$ are the percentiles of the LIDAR point height distribution in a tree segment and also referred to as height dependent variables (Figure 1b). The saliencies $S_i^d = \{d_k\}(k = 1, l)$ are defined as the number of LIDAR points in *l* tree layers from height $((k-1)/l) \cdot h_{tree}$ to height $(k/l) \cdot h_{tree}$ normalized by the total number of LIDAR points in a tree segment (Figure 1c).

The key idea to introduce the third saliency group $S_I = \{S_I^1, S_I^2\}$ is to use the intensity information the waveform decomposition provides for each point. We compute in *l* tree layers with N_k layer points the mean values $I_k^c = \frac{1}{N_k} \sum_{i=1}^{N_k} I_i^c (k = 1, l)$ composing the saliency $S_I^1 = \{I_k^c\}(k = 1, l)$. Additionally, we introduce the saliency $S_I^2 = \{I_{mean}^c\}$ as the overall intensity related value for the entire tree segment.

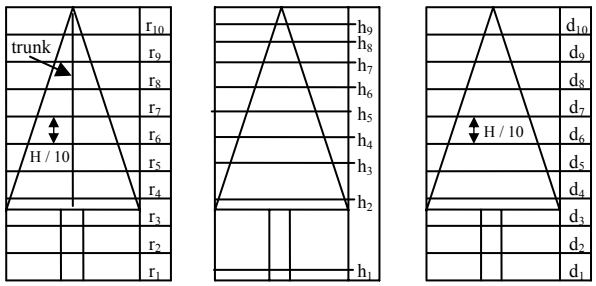

a b c

Figure 1: Tree layers a)-c) Different distributions

3.3 Classification

The tree species classification is a 2-step procedure beginning with a clustering of the tree species and a subsequent Bayes classification. Let $S_t = \{S_g, S_i, S_I\}$ be the salient features of a tree *t* to be classified and let $T_k = \{\mu_k, \Sigma_k\}$ be the density probability model (mean, covariance matrix) of the k^{th} tree class. The probability that a tree *t* is a member of the k^{th} tree class is given by

$$p(S_t|T_k) = \frac{1}{(2\pi)^d \sqrt{|\Sigma_k|}} \exp\left(-\frac{1}{2}(S_t - \mu_k)^T \Sigma_k (S_t - \mu_k)\right) \quad (5)$$

where *d* is the number of saliencies.

The density probability models T_k are found by the Expectation-Maximization algorithm that approximates the distribution of a saliency subset $S \varepsilon S_t$ by

$$p(S) = \sum_{k=1}^{s} \pi_k N(S \mid \mu_k, \Sigma_k) \quad (6)$$

with π_k as the mixing coefficients, $N(S \mid \mu_k, \Sigma_k)$ as the multivariate Gaussian distribution and *s* as the number of

Gaussians. Note, if we just apply the clustering step (6) to the entire set of tree saliencies, we will receive the simple case of an unsupervised tree species classification. Otherwise, step (6) is the learning process of the Bayes classification (5).

4. EXPERIMENTS

Experiments were conducted in the Bavarian Forest National Park that is located in south-eastern Germany along the border to the Czech Republic. The waveform data have been collected by the new full waveform system MK II from TopEye, which is operating at a wavelength of 1550 nm and a PRF of 50 kHz. The scan angle varies within 14 and 20 degrees. The system was flown in late September 2004 at a flying height of 200 m resulting in a nominal point density of approximately 25 points/m^2. Due to the fixed sampling length of 128 samples, the waveform was limited to about 19 m. The sampling rate was 1 GHz providing a vertical resolution to 15 cm. The pulse length of 5 ns created a pulse width with a standard deviation of 25 cm. The emitted Gaussian pulse was not available. Finally, the footprint was 20 cm because of the beam divergence of 1 mrad.

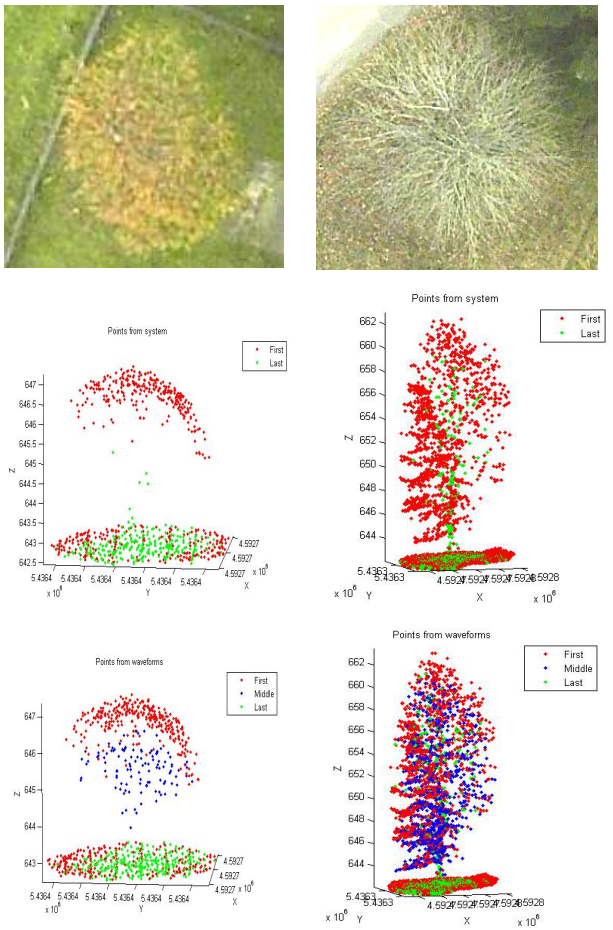

Figure 4: Aerial images of areas 1 and 2 in row 1; Points derived by the TopEye system in row 2, grouped in "First" and "Last" pulse points; Points derived from the waveforms in row 3, grouped in "First" and "Last" pulse points and points between "First" and "Last" pulse (labelled as "Middle" points)

The flown area is of size 500 m x 1700 m and is mainly characterized by Norway Spruce and European Beech. Segmented tree crowns have been derived from a canopy height model (CHM) by a watershed-based algorithm. The CHM was generated from an earlier laser scanning campaign (Heurich et al., 2004). The total number of tree segments amounted to 1000. Reference data for Norway Spruce and European Beech were available in 97 and 23 segments, respectively. In each segment we took the highest tree as the reference tree.

In a first step we applied the waveform decomposition to four sample trees and one meadow area in order to demonstrate the potential of the approach. Firstly, an area of interest was defined in digital orthophotos by manually digitizing a polygon. Secondly, 3D points were generated from all the waveforms intersecting the corresponding prismatic volume segment. The resulting 3D points were grouped into the 3 classes "First", "Last" and "Middle". The classes "First" and "Last" contain all the points derived from the first and last detected peak (t_1, t_{Np}). All the other points referring to t_m ($m = 2, N_p–1$) were classified as "Middle". For comparison, we selected also the first and last pulse points the TopEye system created conventionally with its standard detection procedure. Figure 4 illustrates graphically two sample trees and table 1 contains numerically the number of points extracted by the TopEye system and our waveform decomposition. Note that the single trees 1, 2 and 3 are free-standing. Tree 4 refers to a group of trees in closed forest.

Area		1	2	3	4	5
Tree specie / object type		Deci-duous (leaf-on)	Deci-duous (leaf-off)	Coni-ferous	Deci-duous (leaf-on) and coni-ferous	Mea-dow
Size [m^2]		21.9	72.2	22.2	86.7	28.3
Points from Top-Eye	Total	768	5594	1109	1602	362
	First	503	4168	882	1191	362
	Last	265	1426	227	411	0
Points derived from wave-forms	Total	943	7436	2555	3261	456
	First (%)	553 (59)	4648 (62)	1483 (58)	1678 (51)	456 (100)
	Last (%)	280 (30)	1548 (21)	727 (28)	969 (30)	0 (0)
	Middle (%)	110 (11)	1240 (27)	345 (14)	614 (19)	0 (0)

Table 1: Comparison of points derived by the TopEye system and by the waveform decomposition

Saliency	S_g^1	S_g^2	S_i^h	S_i^d	S_I^1	S_I^2	$S_g^1 + S_I^2$	$S_g^2 + S_I^2$
Conif. [%]	86	94	54	69	79	80	80	80
Decid. [%]	65	65	74	61	65	83	83	82
Total [%]	81	88	58	67	77	81	81	80

Table 2: Overall accuracy of tree species classification

In the next step tree species classification was carried out for the two classes "Coniferous" and "Deciduous" by applying the saliencies $S_t = \{S_g, S_i, S_I\}$ of 1000 tree segments to the unsupervised clustering approach (6). We postponed the

supervised classification with (5) because of the few reference data for European Beech. The overall classification accuracy was derived from the reference data by determining error type I and error type II. We introduced 10 layers for the saliencies S_g^2, S_i^d and S_I^1, and calculated height percentiles for S_i^h in steps of 10%. We only used the last values r_{10} and I_{10} for S_g^2 and S_I^1. Table 2 summarizes the classification results.

5. DISCUSSION

The application of the waveform decomposition to the LIDAR data showed that on average 2 to 3 returns could be detected from a single emitted waveform. Thus, the overall point density of 25 pts/m^2, which is a function of the flying height, the PRF and the flying speed, was increased to roughly 60 pts/m^2.

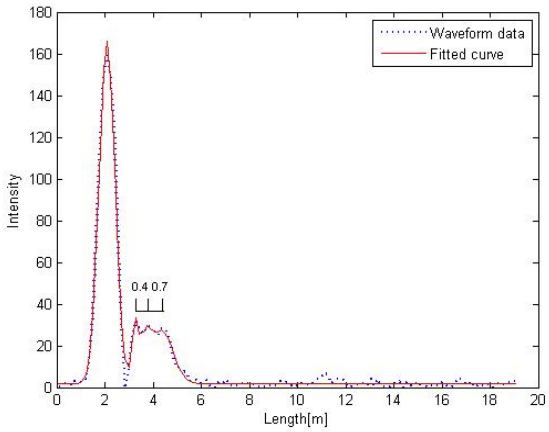

Figure 2: Separated overlaying returns

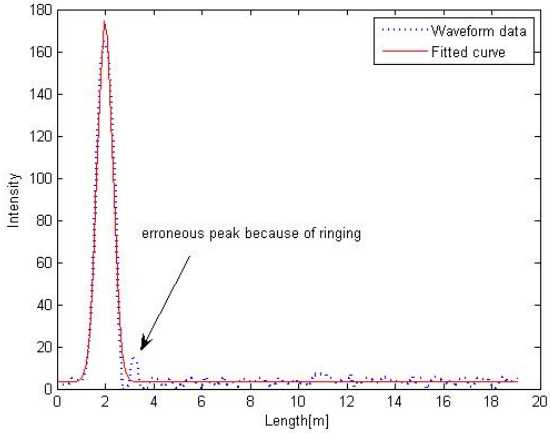

Figure 3: Waveform from a roof with an erroneous peak and the fitted curve where this peak is ignored

Interestingly, the LM iteration scheme (3) successfully separates overlaying returns. Figure 2 shows that three overlaying return pulses could be clearly split up. The corresponding peaks have a distance of 0.4 m and 0.7 m respectively, which is in the order of the nominal height separability derived from the pulse length of 5 ns (Wagner et al. 2003). Note that conventional LIDAR systems can practically discern two return pulses with a distance of about 3 m. Furthermore, the adjustment approach evidences an excellent mean height standard deviation σ_{t_m} of about 2 cm for all points decomposed from the waveforms. This is roughly by the factor 7 better than the nominal height resolution of 15 cm.

Surprisingly, some waveforms contained erroneous peaks that are a typical effect of bandwidth limited receiver electronics called “ringing" and can be observed - most prominently - when the registered light intensity is high. In worst cases there might even occur 2 additional pseudo peaks after the dominant large peak that only results from one reflection. Figure 3 shows a typical example of a waveform resulting from a roof reflection. Two rules have been established to avoid the extraction of pseudo 3D points in that case. The second peak is ignored if it is closer than 1.5 m to the first peak and, secondly, if its amplitude is smaller than 1/5 of the amplitude of the first peak.

Table 1 evidences that the waveform decomposition provides significantly more points than the standard TopEye detection mode. The smallest improvement of about 25% can be observed at tree 1, which is a small deciduous tree in a leaf-on situation. In the area of the coniferous tree 3 the waveform decomposition creates even more than 100% additional points. Two main reasons can be found for this. Firstly, the waveform decomposition decorrelates all the significant returns of the laser beam. Sometimes, up to four or even more points can be found between the first and last peak. Such points are totally ignored by a conventional system. The percentage of the “Middle” points to the total number of decorrelated points varies between 10% and 30%. Secondly, since the waveform decomposition can be flexibly controlled by tuning parameters, it also decorrelates points with a low intensity. Again, many of such points are not registered by a conventional system due to the internal threshold for signal detection. In other words, the higher sensitivity of the waveform decomposition generates much more points. This becomes especially apparent in area 5 (=meadow), where only first pulse points occur.

The classification results of table 2 show, that the saliencies S_g^i describing the crown shape work best for the coniferous trees. Classification just using the saliencies S_i^d and S_i^h representing the internal geometrical structure results in a worse accuracy. The height dependent saliency S_i^h is better for deciduous trees, whereas the density dependent saliency S_i^d works better for coniferous trees. In comparison to this, classification with intensity related saliencies S_I^i yields better results. Especially, the saliency S_I^2 describing the mean intensity value of the segmented tree improves the classification of deciduous trees. However, the saliency S_I^1 describing the intensity related value in the upper tree layer is much worse with 65%. Interestingly, if we combine the best intensity related saliency S_I^2 with the crown shape saliencies S_g the classification results for both tree species is practically the same as with the intensity related saliency S_I^2. Obviously, the classification results are mainly influenced by the crown shape geometry and the mean intensity related value of the tree. Especially, the crown shape drives the classification for coniferous trees considerably. Height and density dependent saliencies are not as good as expected. Probably, the characteristic tree structures are not clearly reflected in these saliencies. The reasons are manifold. Firstly, the waveforms have just a limited length of 19 m and do not penetrate the lower parts of the trees. Secondly, since the data

collection was in September, the beeches were partly in nearly leaf-off or leaf-on situation. Possibly, this caused a different point distribution within one specie. Thirdly, the tree segments resulted from an earlier flight mission with lower point density. In some cases we could observe segments containing for instance several trees or artefacts. Also, smaller trees beneath the tree crown and branches from neighbouring trees may contribute to the tree structure and therefore falsify the saliencies. Notably, we could not clearly identify such cases by introducing a third class as an outlier class. The intensity information turned out to be as the parameter classifying both tree species practically with the same accuracy. Interestingly, just the mean intensity related value S_I^2 yielded the main contribution. Using the values of S_I^1 for all tree height layers resulted in a worse accuracy. Possibly, the number of detected return pulses was too small for the individual layers.

6. CONCLUSIONS

The presented study results show clearly the potential of full waveform data for the comprehensive analysis of tree structures. The number of extracted points is much larger if compared to conventional systems. Future research should evaluate (i) new saliencies for tree species classification based on the 3D points and the waveform signal, which clearly reflect micro structures of the trees like the stem and branches, (ii) waveform data with unlimited length, (iii) influence of point density and (iv) classification of tree sub classes.

7. REFERENCES

Aulinger, T., Mette, T., Papathanassiou, K.P., Hajnsek, I., Heurich, M., Krzystek, P. 2005. Validation of heights from interferometric SAR and LIDAR over the temperate forest site "Nationalpark Bayerischer Wald. *POLINSAR Workshop*, 17th - 20th January, Rome, Italy.

Baltsavias M., Grün, A., Küchler, M., Thee, P., Waser, L.T., Zhang, L. 2006. Tree height measurements and tree growth estimation in a mire environment using digital surface models. *International Workshop "3D Remote Sensing in Forestry", 14 - 15th February, University of Natural Resources and Applied Life Sciences*, 13 -15th, February, Vienna.

Heurich, M., Weinacker, H., 2004. Automated Tree Detection and Measurement in Temperate Forests of Central Europe Using Laserscanning Data. *Proceedings of the ISPRS working group VIII/2 Laser-Scanners for Forest and Landscape Assessment,* Volume XXXVI, PART 8/W2, 3 – 6th October, Freiburg, pp. 198 – 203.

Hofton, M., Minster, J., Blair. J.B. 2000. Decomposition of Laser Altimeter Waveforms. *IEEE Transactions on Geoscience and Remote Sensing*, 38:1989-1996.

Holmgren, J. 2003. Estimation of Forest Variables using Airborne Laser Scanning. Doctoral thesis, *Swedish University of Agricultural Sciences*, Umea.

Hyyppä, J., Hyyppä, H., Litkey, P., Yu, X., Haggren, H., Rönnholm, P., Pyysalo, U., Pikänen, J., Maltamo, M., 2000. Algorithms and Methods of Airborne Laser Scanning for Forest Measurements. *Proceedings of the ISPRS working group VIII/2 Laser-Scanners for Forest and Landscape Assessment,* Volume XXXVI, PART 8/W2, 3 – 6th October, Freiburg, pp. 82 – 89.

Hyyppä, J., Hyyppä, H., Inkinen, M., Engdahl, M., Linko, S., Zhu.Y. , 2000. Accuracy comparison of various remote sensing data sources in the retrieval of forest stand attributes. *Forest Ecology and Management*, 128:109-120.

Jutzi B., Stilla U. 2005. Waveform processing of laser pulses for reconstruction of surfaces in urban areas. *In: Moeller M, Wentz E (eds) 3th International Symposium: Remote sensing and data fusion on urban areas, URBAN 2005. International Archives of Photogrammetry and Remote Sensing.* Vol 36, Part 8 W27.

Levenberg, K. 1944. A method for the Solution of certain non-linear problems in least-squares. *Quart. Appl. Math. 2*, pp 164-168.

Marquardt, D. W. 1963. An algorithm for least-squares estimation of nonlinear parameters. *J. Soc. Indust. Appl. Math. 11*, pp 413-441.

Naesset, E. 2004. Practical Large-scale Forest Stand Inventory Using a Small-footprint Airborne Scanning Laser. *Scandinavian Journal of Forest Research 19*, pp. 164 – 179.

Persson, Å, Söderman, U., Töpel, J., Ahlberg, S. 2005. Visualization and analysis of full-waveform airborne laser scanner data. *In The International Archives of the Photogrammetry, Remote Sensing and Spatial Information Sciences*, Enschede, Netherlands, Vol. XXXVI, Part 3/W19, pp. 103-108.

Persson, A., Holmgren, J., Södermann U., Olsson, H. 2004. Tree species Classification of individual trees in Sweden by Combining High Resoluion Laser Data with High Resolution Near-Infrared Digital Images. *Proceedings of the ISPRS working group VIII/2 Laser-Scanners for Forest and Landscape Assessment,* Volume XXXVI, PART 8/W2, pp. 204-207, 3 – 6th October, Freiburg.

Reigber, A., 2001. Airborne Polarimetric SAR Tomography, *DLR Forschungsbericht No. 2002-2*, Doctor thesis, Stuttgart University.

Rousseeuw, P.J., Leroy, A.M. 1987. Robust Regression and Outlier Detection, *Wiley-Interscience, New York (Series in Applied Probability and Statistics)*, 329 pages. ISBN 0-471-85233-3.

Wagner, W., Ullrich, A., Briese, C. 2003. Der Laserstrahl und seine Interaktion mit der Erdoberfläche. *Österreichische Zeitschrift für Vermessung und Geoinformation (VGI)*, 91(4); 223 - 235.

8. ACKNOWLEDGEMENTS

We thank the Administration of Bavarian Forest National Park to give us the opportunity to use the possibilities of their remote sensing test sites. Also, the laser measurements were financed by the Administration of Bavarian Forest National Park. We also like to thank Hakan Sterner and the staff at TopEye AB for delivering a high quality laser data set.

This research has been funded by the German Department of Education and Research (BMBF) under the contract number 17311B04.